Received 9 February 2006
Revised 30 October 2006
Accepted 8 January 2007

# Assessment of a zero-dimensional model of tumble in four-valve high performance engine

Damian Ramajo, Angel Zanotti and Norberto Nigro
*International Center for Computational Methods in Engineering, INTEC-Universidad Nacional del Litoral-CONICET, Santa Fe, Argentina*

## Abstract

**Purpose** – The purpose of this paper is to assess a phenomenological zero-dimensional model (0-D model) in order to evaluate both the in-cylinder tumble motion and turbulence in high-performance engine, focusing on the capability and sensitivity of the model.

**Design/methodology/approach** – The study was performed using a four-valve pentroof engine, testing two different intake ports. The first one was a conventional port and the second one was design in such a way to promote tumble. CFD simulations for admission and compression strokes under different engine conditions were carried out. Then, the in-cylinder entrance mass and mean velocities from CFD were imposed as boundary conditions in the 0-D model.

**Findings** – Marked discrepancies between 0-D model and CFD results were found. As expected, for the original port, CFD results displayed a poor tumble generation during the admission period. It was followed by a fast degradation of the tumble momentum along the compression stroke due to it was not dominant over the other two momentum components. 0-D model overestimated the entrance-tumble but underestimated the vortex degradation along the compression stroke, resulting in higher tumble predictions, thereby it is not recommended for low-tumble engines. As for the modified port, 0-D model assumptions were closer to the in-cylinder flow field from CFD, but results underestimated the entrance-tumble during the intake stroke and predicted excessive tumble at the end of the compression stroke. Summarizing, 0-D model neither showed sensitivity to changes in the intake port because of the scarce information about the entrance-flow field nor it was not suitable to evaluate the tumble degradation.

**Originality/value** – The limitations of the current model were highlighted, given possible guidelines in order to improve it.

**Keywords** Engine components, Turbulence, Simulation

**Paper type** Research paper

## Introduction

In-cylinder charge motion in high-performance heat engines is one of the main factors affecting the engine behavior. In two-valve engines, the charge motion can be characterized by a vortex motion called swirl; the flow enters through the inlet valve and turns around the cylinder axis guided by the cylinder walls. In four-valve engines, valves have a symmetric configuration with respect to the cylinder mean plane.

The authors would like to express their gratitude to Professor Stephen Benjamin of Coventry University, UK, for his valuable advice during this study. This work has received financial support from Concejo Nacional de Investigaciones Científicas y Técnicas (CONICET, Argentina, grant PIP – 02552/2000) and ANPCyT (Argentina, grants PICT 12-14573/2003 (Lambda), PME 209/2003 (Cluster) and PID 398/03 (DIVA)).

International Journal of Numerical Methods for Heat & Fluid Flow
Vol. 17 No. 8, 2007
pp. 770-787

0961-5539
DOI 10.1108/09615530710825765

This causes the flow to turn around an axis normal to the cylinder axis. This motion, called tumble, is the most important vortex structure generated inside four-valve engines. This is also true for three-and five-valve engines (Li *et al.*, 2003; Lee *et al.*, 2001). Tumble vortexes are created during the intake stroke and they are degraded along the compression stroke increasing the turbulent kinetic energy $k$ of the flow (Kang and Baek, 1995; Kang and Baek, 1998; Li *et al.*, 2001a, b; Ramajo *et al.*, 2005). It produces a well-known improvement in combustion efficiency because high-turbulence level leads to better charge mixing (McLanddress *et al.*, 1996) and greater burning speeds (Aleiferis *et al.*, 2004).

Many researchers have made in-cylinder experimental measurements in order to quantify the tumble motion and turbulence levels (Kang and Baek, 1995; Kang and Baek, 1998; Li *et al.*, 2001a; Lee *et al.*, 2001). However, there is little work reporting numerical studies of this flow patterns (Li *et al.*, 2001a; McLanddress *et al.*, 1996; Lee *et al.*, 2001; Huang *et al.*, 2005), and hardly any using zero-dimensional models (0-D models) to approach charge motion and turbulence (Poulos and Heywood, 1983; Benjamin, 1993; Achuth and Metha, 2001). Incorporating the in-cylinder charge motion in a zero-dimensional engine simulator allows taking into account the effect of the main parameters related to the geometry of valves and combustion chamber, which have strong incidence in the intake and compression processes.

In this paper, a 0-D model to predict tumble and turbulence in four-valve pentroof engines is analyzed and assessed by comparison with CFD results. This model was first introduced by Benjamin (1993) to study the evolution of tumble and turbulence during the compression stroke in disk combustion chambers. The model was formulated based on a mean flow analysis of tumble motion in conjunction with a $k$-$\varepsilon$ scheme for turbulence. The model formulation assumes the existence of a macro vortex of tumble and uses the angular-momentum conservation equation to estimates the vortex speed. The model was later extended by Achuth and Metha (2001) by introducing two additional geometrical parameters: the pentroof-chamber angle $\theta$ and the valve seat angle $\beta$, to take into account the tumble motion and turbulence generation occurring along the intake stroke.

Even though the present work is focused on the 0-D model, a summarized description of the CFD simulations used to validate this model is also provided. A more detailed description of CFD implementation can be found in the references (Ramajo *et al.*, 2005).

## 0-D model description

The 0-D model has a phenomenological basis and it includes terms for the turbulent kinetic energy $k$ and the angular momentum $J$ generated during the in-cylinder charge induction in four-valve pentroof engines.

The model may be divided in two main sub models, the tumble one and the turbulence one.

### *Tumble model*

Tumble formulation assumes that the inlet flow has angular momentum with respect to an axis normal to the cylinder axis, which contributes to a tumble vortex centred in the middle of the cylinder. The vortex speed is computed by solving a macroscopic angular momentum conservation equation:

$$\frac{dJ}{dt} = \frac{dJ_{in}}{dt} - T_s - T_w, \tag{1}$$

where $J_{in}$ is the torque source given by the incoming flow through the inlet valves and $T_s$ and $T_w$ are momentum losses due to internal shear stresses and wall friction, respectively. $J_{in}$ is computed by considering that the inlet flow enters with a velocity $U_O$ transporting a positive angular momentum with respect to a theoretical tumble vortex centre:

$$\frac{dJ_{in}}{dt} = \dot{m}_{in} U_0 h, \tag{2}$$

being $h$ the height from the instantaneous vortex centre to the valve head (Figure 1) and $\dot{m}_{in}$ is the mass flow rate through the inlet valves. $U_O$ is defined from the incoming mean flow speed $u_{in}$ (ratio between $\dot{m}_{in}$ and the instantaneous curtain area):

$$U_0 = c_v u_{in} \cos(\theta - \beta). \tag{3}$$

The coefficient $c_v$ in equation (3) must be taken as 0.5 or 1 depending on the instantaneous inlet-valve lift $L_v$. Achuth and Mehta recommended to use 0.5 when $L_v < L_{v\max}/2$ and 1 when $L_v \geq L_{v\max}/2$ ($L_{v\max}$ being the maximum inlet-valve lift).

0-D model assumes that the tumble macro vortex has an ellipsoidal shape, which is bounded by the whole cylinder. Then, the vortex velocity field is defined as two-dimensional as a function of a characteristic tumble velocity $U$ as follow:

$$u_x = 2U\left(1 - \frac{z^2}{R^2}\right)\frac{y}{L}, \quad u_y = -2U\left(1 - \frac{z^2}{R^2}\right)\frac{x}{W}, \tag{4}$$

where $R$ is the cylinder radius, $L$ is the instantaneous chamber height (from the piston head to the uppermost point of the chamber) and $W$ is the width of an elemental vortex (Figure 1). The velocity profile given by equation (4) implies that the fluid velocities on the piston and cylinder heads are the same. This motivates a division of the domain boundaries in two zones. The first one is composed by the cylinder walls (cyl zone), and the second one by the piston and cylinder heads (p zone).

Shear stress estimation at walls is done by the application of the well-known solution for the friction force between parallel plates:

$$\tau_w = \frac{1}{2}\rho u_w^2 c_f, \tag{5}$$

where $u_w$ is the flow velocity outside the turbulent boundary layer and it is valued as $U$ in the present model. The friction coefficient $c_f$ is obtained by the following correlation:

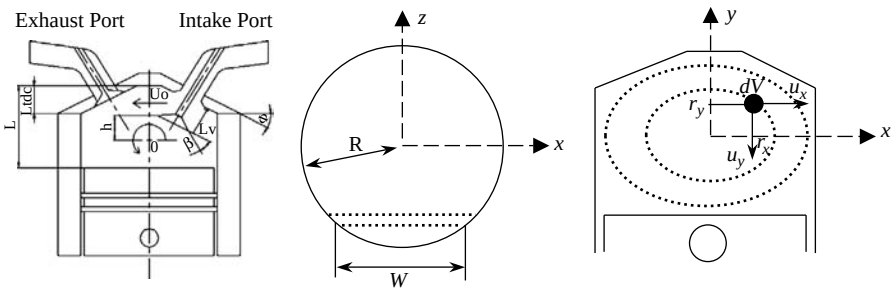


**Figure 1.**
Cylinder geometry and 0-D model parameters

$$c_f = 0.074Re^{-0.2} \text{ with } Re = \frac{2RU}{\nu} \quad (5\times10^5 < Re < 10^7), \tag{6}$$

where $\nu$ is the kinematics viscosity.

The torque $T_w$ arises from the integration of $\tau_w$ over each surface in both zones (p and cyl zones), being:

$$T_w = L\int_{sup}\tau_w\,dA = L\left(\int_{cyl}\tau_w\,dA_{cyl} + \int_{p}\tau_w\,dA_p\right) = 0.72c_f mU^2, \tag{7}$$

where $m$ is the instantaneous in-cylinder mass. On the other hand, $T_s$ is obtained by integration of the shear stresses $\tau_s$. For a Newtonian fluid $\tau_s$ are computed as:

$$\tau_{xy} = \rho\nu_t\left(\frac{\partial u_y}{\partial x} + \frac{\partial u_x}{\partial y}\right) \quad \text{and} \quad \tau_{yz} = \rho\nu_t\frac{\partial u_y}{\partial z} \text{ with } \nu_t = \frac{c_d k^2}{\varepsilon}, \tag{8}$$

where $\nu_t$ is the turbulent viscosity and $C_d$ is an empirical coefficient equal to 0.09. The velocity gradients in the above equations are computed from equation (4). Finally, $T_s$ is written as:

$$T_s = L\int_{sup}\tau_s\,dA = L\left(\int_{cyl}\tau_s\,dA_{cyl} + \int_{p}\tau_s\,dA_p\right) = \frac{3Um\nu_t}{2}\left(\frac{1}{L} + \frac{8}{9\pi R}\right). \tag{9}$$

Concluding, the final expression for the tumble dynamics is obtained by replacing the expressions for $dJ_{in}/dt$, $T_s$ and $T_w$ from equations (2), (7) and (9) into equation (1):

$$\frac{d}{dt}\left[\frac{mU}{8}(L + 1.81R)\right] = \dot{m}_{in}U_0 h - \frac{3}{2}Um\nu_t\left(\frac{1}{L} + \frac{8}{9\pi R}\right) - 0.72c_f mU^2. \tag{10}$$

With a little algebra, equation (10) can be derived getting an expression for the tumble velocity rate as:

$$\dot{U} = \frac{8}{m(L+1.81R)}\left\{\dot{m}_{in}U_0 h - \frac{3}{2}Um\nu_t\left(\frac{1}{L} + \frac{8}{9\pi R}\right) - 0.72c_f mU^2 - \frac{(L+1.81R)}{8}U\dot{m} - \frac{mU\dot{L}}{8}\right\}. \tag{11}$$

In equation (11), $\dot{m}_{in}$ is the inlet mass flow rate and $\dot{m}$ is the net mass flow rate in-cylinder.

*Turbulence model*

The turbulence intensity $u'$ is a useful parameter to quantify the turbulence level. It may be obtained straightforwardly from a zero-dimensional $k$-$\varepsilon$ model. It takes into account the incoming turbulence due to the inlet flow and the turbulence production from the tumble vortex degradation during the compression stroke. Destruction of the mean vortex gives rise to turbulence enhancement, as it supplies the mean flow energy contained in the vortex. Achuth and Metha (2001) describe three different stages of turbulence; the first one is the intake generated turbulence, then a tumble enhanced turbulence and finally a turbulence decay phase. During the intake, the turbulent

kinetic energy may reaches a peak depending upon valve geometry and in-cylinder flow conditions before bottom dead centre (BDC), decreasing further than the BDC. The tumble enhanced stage is characterized by shear deformation, the spin-up of the vortex and the eventual vortex breakdown. For that reason, the turbulent kinetic energy reaches a second peak close to the top dead centre (TDC). So, the shear stresses arising from vortex breakdown seem to be the major source of turbulence from tumble. Finally, the third stage is associated with a fast increase of dissipation rate with the consequent turbulence decay at the end of the compression stroke (Benjamin, 1993; Ramajo *et al.*, 2005).

Regarding the zero-dimensional $k$-$\varepsilon$ model, it has been deduced from a generic transport equation for a turbulent variable $s$. It includes a production term $P_s$, a dissipation term $D_s$ and a turbulent diffusion term $G_s$:

$$\frac{\mathrm{d}s}{\mathrm{d}t} = P_s - D_s + G_s. \tag{12}$$

To write the balance equations for $k$ and $\varepsilon$ in a zero-dimensional framework, all variables must been spatially averaged inside the cylinder. Resulting expressions for $\dot{k}$ and $\dot{\varepsilon}$ are:

$$\begin{aligned}\dot{k} = &-\frac{2}{3}\frac{\dot{L}}{L}k + \frac{5}{2}\upsilon_t U^2\left[\frac{1}{L^2} + \frac{7}{15R^2} - \frac{256}{75\pi RL}\right] \\ &- \varepsilon - 2\left[\frac{\upsilon_{t,\mathrm{eq-cyl}}(k - k_{\mathrm{eq-cyl}})}{\mathrm{Ry}_{\mathrm{eq-cyl}}} + \frac{\upsilon_{t,\mathrm{eq-p}}(k - k_{\mathrm{eq-p}})}{\mathrm{Ly}_{\mathrm{eq-p}}}\right] + \frac{\dot{m}_{\mathrm{in}}}{m}(k_{\mathrm{in}} - k),\end{aligned} \tag{13}$$

$$\begin{aligned}\dot{\varepsilon} = &-\frac{4}{3}\frac{\dot{L}}{L}\varepsilon + \frac{5}{2}\upsilon_t U^2\left[\frac{1}{L^2} + \frac{7}{15R^2} - \frac{256}{75\pi RL}\right]\frac{c_{\varepsilon 1}\varepsilon}{k} \\ &- \frac{\varepsilon^2}{k}c_{\varepsilon 2} - 2\left[\frac{\nu_{t,\mathrm{eq-cyl}}(\varepsilon - \varepsilon_{\mathrm{eq-cyl}})}{\mathrm{Ry}_{\mathrm{eq-cyl}}} + \frac{\nu_{t,\mathrm{eq-p}}(\varepsilon - \varepsilon_{\mathrm{eq-p}})}{Ly_{\mathrm{eq-p}}}\right] + \frac{\dot{m}}{m}(\varepsilon_{\mathrm{in}} - \varepsilon),\end{aligned} \tag{14}$$

where $k_{\mathrm{in}}$ and $\varepsilon_{\mathrm{in}}$ are given by:

$$k_{\mathrm{in}} = (c_k u_{\mathrm{in}})^2 \quad \varepsilon_{\mathrm{in}} = \frac{c_d k_{\mathrm{in}}^{3/2}}{c_l L_{v\max}}. \tag{15}$$

$c_k$, $c_l$, $c_{\varepsilon 1}$ and $c_{\varepsilon 2}$ coefficients are 0.47, 0.30, 1.44 and 1.92, respectively. By evaluating the wall turbulence flow, the model adopts averaged velocities $u_{\mathrm{cyl}}$ and $u_{\mathrm{p}}$ on each boundary zone. Those velocities are given by integrating equation (4) on each one of them:

$$u_{\mathrm{cyl}} = \frac{1}{2}U \quad \text{and} \quad u_{\mathrm{p}} = \frac{3}{4}U. \tag{16}$$

The friction velocity $u^*$ is used to obtain the equilibrium turbulent kinetic energy $k_{\mathrm{eq}}$. In each zone, $u^*$ arises from their respective frictional coefficients $c_{f-\mathrm{p}}$ and $c_{f-\mathrm{cyl}}$ (given in equation (6)):

$$u^*_{\mathrm{cyl}} = u_{\mathrm{cyl}}\left(\frac{c_{f_{\mathrm{cyl}}}}{2}\right)^{\frac{1}{2}} \quad \text{and} \quad u^*_{\mathrm{p}} = u_{\mathrm{p}}\left(\frac{c_{f_{\mathrm{p}}}}{2}\right)^{\frac{1}{2}}. \tag{17}$$

Finally, the equilibrium expressions for the turbulent kinetic energy $k_{eq}$, the eddy dissipation rate $\varepsilon_{eq}$ and the turbulent viscosity $\nu_{eq}$ at a distance $y_{eq}$ from the walls are given by:

$$k_{eq} = \frac{(u^*)^2}{(c_d)^{\frac{1}{2}}}, \quad y_{eq} = \frac{\nu}{u^*} \exp\left(0.41\left(\frac{2}{c_f}\right)^{\frac{1}{2}} - 5\right), \quad \varepsilon_{eq} = \frac{(u^*)^3}{0.41 y_{eq}} \quad \text{and} \quad \nu_{t_{eq}} = c_d \frac{k^2}{\varepsilon_{eq}}. \tag{18}$$

Then, the turbulence level predicted by the $k$-$\varepsilon$ model can be expressed by means of the turbulence intensity $u'$ defined as:

$$\acute{u} = \sqrt{\frac{2k}{3}}. \tag{19}$$

## Methodology

CFD simulations were performed using ANSYS CFX 5.7 software. Two different port configurations were implemented, the first one using a conventional intake port (conventional port or port 1) and the second one using a special port to promote tumble (tumble port or port 2). Both configurations are shown in Figure 2 and the engine data are given in Table I.

The 0-D model was implemented in Fortran 90. The equation system (equations (10), (13) and (14)) was integrated in time using a simple Backward Euler scheme with a constant time step equivalent to 0.1 crank angle (CA).

In order to do a more realistic comparison between the 0-D model and the CFD predictions the instantaneous mass flow rate from CFD simulations (Figure 3) were imposed to the 0-D model during the intake period.

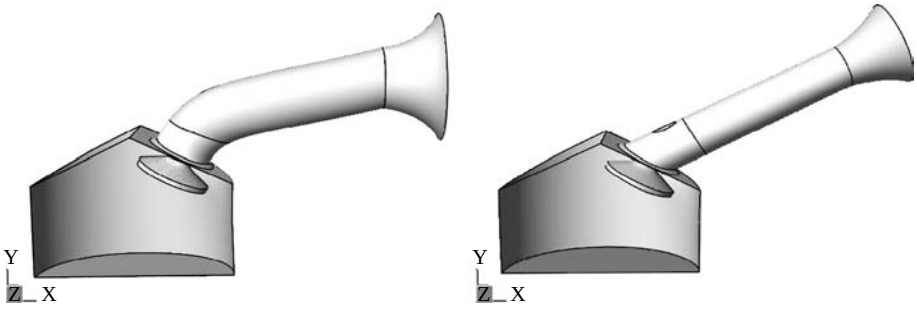


**Figure 2.**
Left: conventional port; right: tumble port

| | | | |
|---|---|---|---|
| Cylinder radius (mm) | 40 | Valve seat angle (deg) | 25 |
| Stroke (mm) | 80 | Inlet valve diameter (mm) | 30 |
| Connecting rod length (mm) | 155.4 | Valve stem diameter (mm) | 6 |
| Compression ratio | 10.1 | Maximum valve lift (mm) | 10 |
| Pentroof angle (deg) | 25 | Valve open angle BTDC (deg) | 10 |
| Engine speed (rpm) | 1,500-2,500 | Valve close angle ABDC (deg) | 36 |

**Table I.**
Engine parameters

The angular momentum $J$ was chosen as a comparative parameter for the vortex motion. $J$ from CFD results was easily obtained from the velocity fields inside the cylinder by assuming a Cartesian reference frame placed at the instantaneous cylinder centre. On the other hand, the angular momentum from the 0-D model results was obtained from the characteristic tumble velocity $U$, integrating the assumed velocity field (given by equation (4)) inside an ellipsoidal domain bounded by the combustion chamber walls by means of:

$$J_{nz} = \frac{\rho \int (-u_x r_y + u_y r_x) \mathrm{d}V}{m} = \frac{3}{8,960} U(175\pi R + 256L), \tag{20}$$

where $J_{nz}$ is the $z$ component of the angular momentum (tumble movement), which is normalized with respect to the current mass inside the cylinder ($m$) and $r_x$ and $r_y$ are the coordinates from the $z$-axis to each differential volume $\mathrm{d}V$ inside the ellipsoidal domain (Figure 1).

*CFD simulation details*

CFX 5.7 allows the simulation of problems involving time-dependent domain changes by moving the mesh following imposed motion laws at boundary walls. However, engine simulations imply extreme boundary displacements, so it is necessary to choose a motion strategy. There are at least two possibilities; either do not use remeshing and develop a numerical scheme that can withstand highly distorted elements or use a remeshing procedure (Johan *et al.*, 2001). Strong mesh distortions are not supported by the software and moreover, they may degrade the quality of the numerical solution. For that reasons, it was chosen the later strategy. CFD simulations were performed by dividing both the intake and compression strokes in five stages of 36° of CA each one. Inside each interval, the geometry was redrawn and remeshed and each stage was initialized from the previous results, via interpolation (of course, it can add some extra diffusion over the solution during each interpolation).

Simulations started from the TDC, $\varphi = 0°$ and reached the $\varphi = 360°$ at the end of the compression stroke, being $\varphi$ the CA. In each stage, the instantaneous valve lift was provided by a polynomial function and the piston displacement $d_\mathrm{p}$ was imposed by the well known crank-slider mechanism expression:

$$d_\mathrm{p} = l + a - \left[a\cos\varphi + \left(l^2 - a^2\sin^2\varphi\right)^{\frac{1}{2}}\right], \tag{21}$$

where $l$ is the connecting rod length and $a$ is the crankshaft radius.

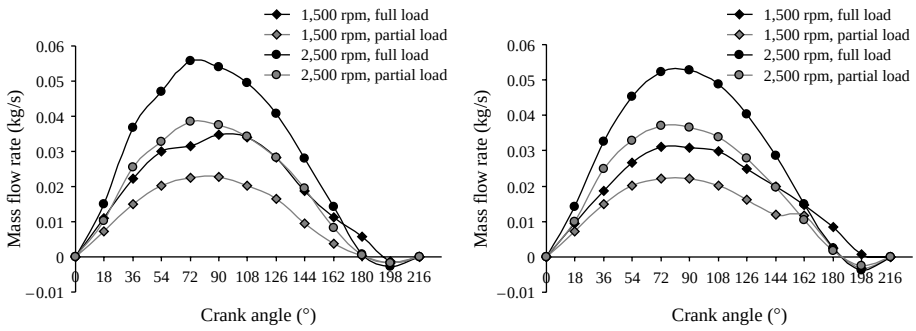


**Figure 3.**
Mass flow rate obtained from CFD; left: conventional port; right: tumble port

An open boundary condition with a constant static pressure was used at the inlet. Two inlet load levels were considered, a full load condition by imposing a pressure of one atmosphere and a partial load condition with a pressure of 0.7 atmospheres. Air (ideal gas) was chosen as working fluid. A no-slip boundary condition and a smooth roughness were imposed in all walls. The initial conditions were a homogeneous pressure equal to the inlet pressure, a null flow velocity and a temperature of 300 K in all points of the domain.

The Navier-Stokes equations for a compressible flow were integrated using a backward Euler scheme with a constant time step corresponding to 3.6° CA. A RMS tolerance of 1e-4 was used as convergence criterion. A standard $k$-$\varepsilon$ model with a wall law was used to reproduce turbulence phenomena. Owing to the symmetrical valve configuration and the selected turbulence model, it was possible to simulate only half of the full cylinder geometry.

The heat transfer between the fluid and the boundaries was included. A temperature of 450 K was imposed to the cylinder and the inlet-duct walls. A higher temperature of 600 K was considered for the valve, the piston, and the cylinder-head walls.

An unstructured tetrahedral mesh was employed to represent the geometry. A refinement around the valve and cylinder head zones to capture the vortexes and the small flow structures generated over the valve-unloading zones was used. The maximum mesh size used was 0.5 mm around the valve region rising to 3 mm far from it. The maximum amount of mesh elements varied from around 300,000 to more than 700,000 depending on the instantaneous piston and valve locations. In Figure 4, the conventional port surface mesh corresponding to the beginning of the second stage (36° to 72° CA ATDC) is shown.

## Results and discussion

Figure 5 shows the normalized tumble momentum $J_{nz}$, at left for the conventional port configuration and at right for the tumble one, obtained by CFD and 0-D model simulations.

As for the conventional port, only scarce agreement can be seen. Estimations for 0-D model are closer to CFD results only during the first middle of the intake stroke while valve is opening. After maximum valve lift is reached the 0-D model tends to overestimate the tumble motion. But, the tumble dissipation rate, measured in terms of the slope of that curve, during the compression stroke seems to be similar to CFD results.

As regards the tumble port configuration, the 0-D model fails to predict tumble generation during the intake stroke, underestimating the tumble along all the intake and compression strokes, except for the latter's end.

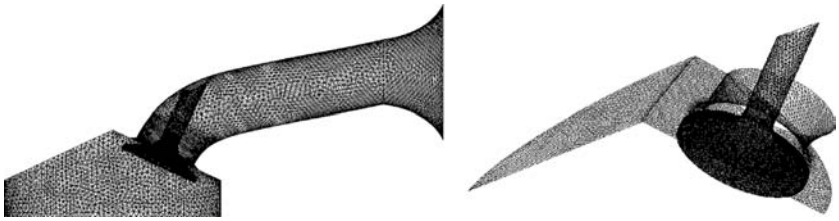

**Figure 4.**
Surface mesh (conventional port); left: full domain; right: cylinder head and valve zones

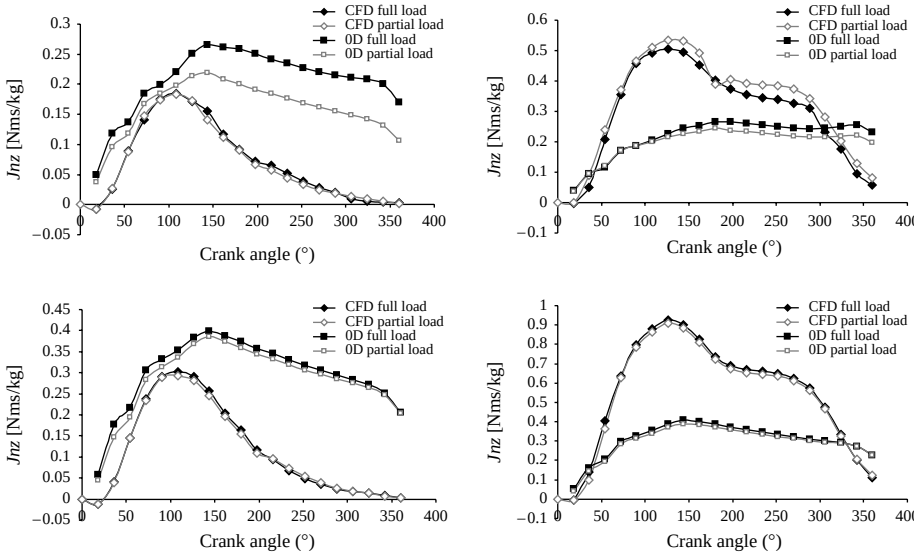


**Figure 5.**
Normalized tumble momentum $J_{nz}$ from 0-D model and CFD simulations (left: conventional port, right: tumble port); upper: engine speed of 1,500 rpm; bottom: engine speed of 2,500 rpm

It must be pointed out that port-configuration changes have strong incidence in tumble generation. It was found both in experimental (Kang and Baek, 1995) and also in CFD works (McLanddress *et al.*, 1996; Li *et al.*, 2001b; 2003; Lee *et al.*, 2001; Ramajo *et al.*, 2005; Seeley, 1998) that tumble momentum can be largely increased by driving the inlet flow in such a way to generate a more defined flow structure that remains until the end of the compression stroke. But, as it can be noted in Figure 5, those changes are not apparent in the 0-D model results. Although the 0-D model includes some engine features ($\theta$ and $\beta$ parameters), it is easy to find out that it has not enough sensitivity to changes in the port configuration, because the model has not the capability to predict the upstream-valve flow behaviour.

Although Achuth and Metha (2001) recommend to use a calibration point to improve the 0-D model results (this correction is made by scaling the 0-D model results for a scale factor taken as the ratio between the calibration value and the 0-D model result at BDC), it does not seem to have a benefic over the tumble predictions during the intake stroke, as is shown in Figure 6.

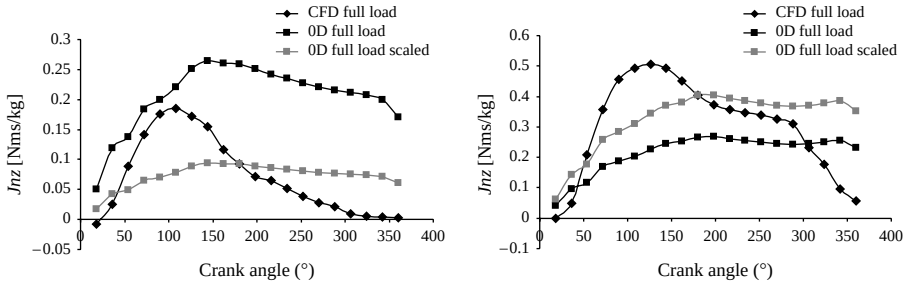


**Figure 6.**
Normalized tumble momentum $J_{nz}$ from 0-D model and CFD simulations for engine speed of 1,500 rpm; left: conventional port; right: tumble port

Tumble port configuration generates stronger tumble momentum than the conventional one. In fact, the tumble component dominates the other two angular momentum components in the former, as shown in Figure 7. It must be noted that if a symmetrical flow behaviour is considered (CFD simulations were performed only over half of the full cylinder), both $J_{nx}$ and $J_{ny}$ become zero when they are integrated in the full cylinder.

CFD simulations for both ports show marked differences in the velocity field over the inlet valve curtain (Figure 8). A quantitative analysis of the intake mass flow rate also confirms it. On the one hand, for the conventional port the inlet flow is strongly deviated by the valve and seat-valve surfaces. This means that flow distribution around the valve curtain is almost homogeneous. For some piston positions this equalized mass flow rate around the valve curtain may cause a negative interference in the angular momentum that tends to reduce the incoming tumble. On the other hand, for the tumble port the inlet flow has a definite direction formed by the relative angle between the inlet duct and the valve axis. The wake produced by the stem is an evidence of the main orientation of the incoming flow in relation to the valve axis, as it is shown in Figure 8. This has a marked incidence in the amount of tumble motion entering though the inlet valve. This means that a strong positive tumble component may be obtained with this modified port configuration because almost the overall inlet mass flow generates positive tumble for higher valve lifts.

The incoming mass flow rate, its angular momentum, and its orientation seem to play an important role in the prediction of the tumble dynamics. Owing to this fact, a correction of the incoming velocity coming from the CFD results was introduced to

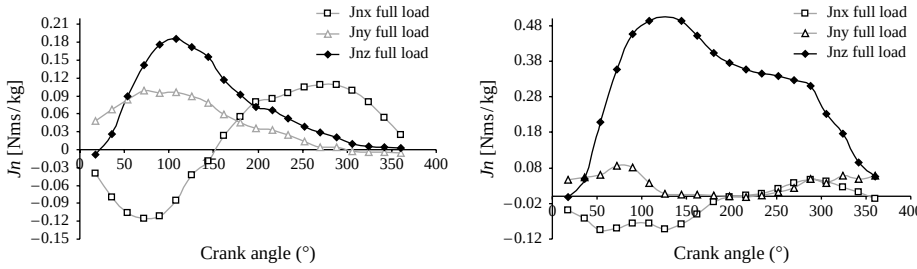


**Figure 7.**
Normalized angular momentum $J_n$ from CFD simulation for both port configurations (left: conventional port, right: tumble port), full load and engine speed of 1,500 rpm

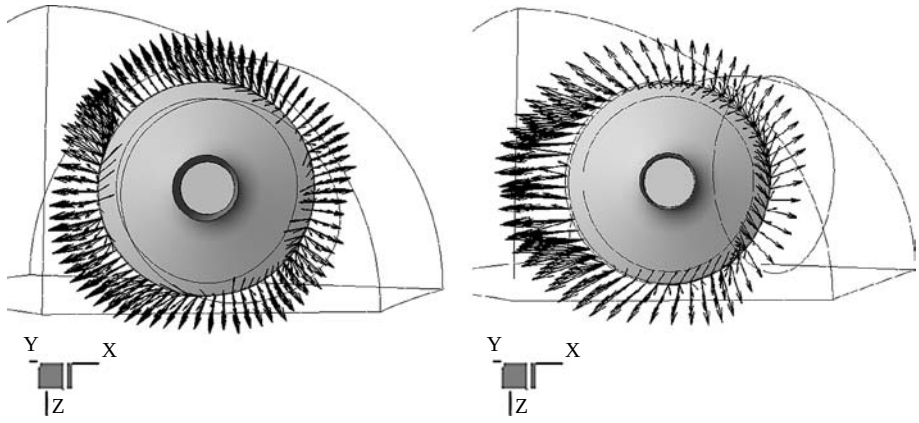


**Figure 8.**
Velocity field over the valve curtain at 8 mm valve lift (engine speed of 1,500 rpm); left: conventional port; right: tumble port

assess the extent to which the 0-D model may improve its angular momentum prediction. To this aim, the flow distribution around the inlet valve was analyzed from the CFD flow field. The valve curtain was divided in two zones (zones 1 and 2) as shown in Figure 9. Then, a parametric analysis by means of a set of coefficients built from flow-velocity averages $\bar{v}$ weighted with the mass flow rate was performed. The expressions for the averaged velocities along with the set of coefficients are given by:

$$\bar{v}_{i,j} = \frac{\sum_{k=1}^{n} v_{k,j}^{i} \dot{m}_k}{\sum_{k=1}^{n} \dot{m}_k}, \quad \bar{v}_i = \left(\overline{v_{ix}}^2 + \overline{v_{iy}}^2 + \overline{v_{iz}}^2\right)^{\frac{1}{2}},$$
$$C_{im} = \frac{\dot{m}_i}{\dot{m}}, \quad C_{iv} = \frac{\bar{v}_i}{\bar{v}_n}, \quad C_{ix} = \frac{\overline{v_{ix}}}{\overline{v_i}}, \quad C_{iy} = \frac{\overline{v_{iy}}}{\overline{v_i}}, \quad \text{and} \quad C_{iz} = \frac{\overline{v_{iz}}}{\overline{v_i}}, \tag{22}$$

where $\overline{v}_{i,j}$ is the averaged $j$-Cartesian component of the velocity at the $i$ curtain zone ($i = 1$ or 2), $v_{k,j}^{i}$ and $\dot{m}_k$ are the $j$-component of the velocity and the mass flow rate at the $k$ point of the mesh over the curtain, $\dot{m}_i$ and $\overline{v_i}$ are the mass flow rate and the averaged total velocity at the $i$ curtain zone, and $\overline{v_n}$ is the mean flow velocity (ratio between the incoming mass flow rate through the valve and the total curtain area).

The coefficients computed using equation (22) are presented in Table II. They can help to explain the improvement in the tumble generation obtained by changing the port configuration.

These coefficients are consistent with Figure 8. As for the conventional port, coefficient $C_{1m}$ shows a more homogeneous flow distribution along all the valve-lift range. In zone 1, the $y$ and $z$ components of the flow ($C_{1y}$ and $C_{1z}$, respectively) are more relevant with respect to the main flow in the $x$ direction. $C_{1x}$ holds closer to 1 for low-valve lifts, but it decreases while valve lift increases. It seems to have a reasonable behaviour because valve surface imposes a stronger flow deviation for low-valve lifts, while for high-valve lifts its influence over the entering flow diminishes. This tendency does not seem to occur in zone 1 for the tumble port configuration, where for all valve-lift ranges the flow finds an easier path to enter the cylinder without suffering strong deflections. With respect to the zone 2, the $x$ component of the flow decays strongly while valve lift increases and flow gets mainly directed in a vertical way. It produces negative tumble momentum.

As regards the tumble port configuration, for high-valve lifts around 80 per cent of the overall mass flow rate enters through the zone 1 with a velocity mostly tangential to the tumble vortex, producing a positive tumble momentum. The coefficient $C_{1x}$ is

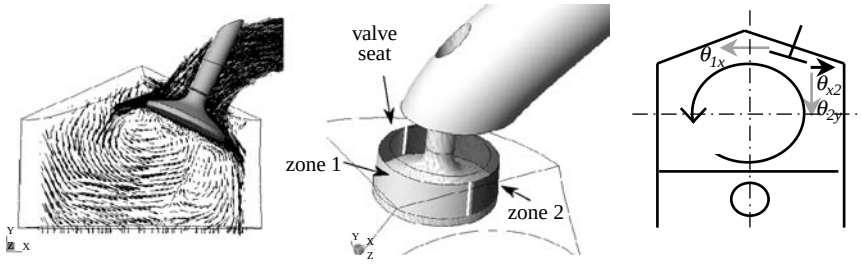


**Figure 9.**
Left: velocity field over the valve mean plane; centre: delimitation of zones over the valve curtain; right: components of flow which induce tumble momentum

| Port | | $L_v$ | $\dot{m}$ | $C_{1m}$ | $C_{2m}$ | $C_{1v}$ | $C_{2v}$ | $C_{1x}$ | $C_{1y}$ | $C_{1x}$ | $C_{2x}$ | $C_{2y}$ | $C_{2x}$ |
|---|---|---|---|---|---|---|---|---|---|---|---|---|---|
| Port 1 | Open | 2 | 0.00835 | 0.53 | 0.47 | 1.17 | 0.90 | 0.99 | 0.02 | 0.12 | 0.57 | 0.81 | 0.15 |
| | | 4 | 0.01130 | 0.59 | 0.41 | 1.54 | 1.24 | 0.97 | 0.23 | 0.11 | 0.24 | 0.97 | 0.05 |
| | | 6 | 0.01407 | 0.60 | 0.40 | 1.66 | 1.32 | 0.96 | 0.26 | 0.10 | 0.22 | 0.97 | 0.07 |
| | | 8 | 0.01461 | 0.64 | 0.36 | 2.00 | 1.43 | 0.95 | 0.31 | 0.10 | 0.16 | 0.98 | 0.10 |
| | | 10 | 0.01446 | 0.63 | 0.37 | 2.49 | 1.85 | 0.92 | 0.38 | 0.13 | 0.20 | 0.97 | 0.12 |
| | Close | 8 | 0.01337 | 0.58 | 0.42 | 1.99 | 1.51 | 0.93 | 0.32 | 0.20 | 0.30 | 0.95 | 0.08 |
| | | 6 | 0.01172 | 0.56 | 0.44 | 1.66 | 1.33 | 0.94 | 0.29 | 0.15 | 0.34 | 0.94 | 0.01 |
| | | 4 | 0.00869 | 0.55 | 0.45 | 1.53 | 1.34 | 0.96 | 0.26 | 0.11 | 0.39 | 0.92 | 0.04 |
| | | 2 | 0.00367 | 0.55 | 0.45 | 1.22 | 1.08 | 0.97 | 0.19 | 0.14 | 0.48 | 0.87 | 0.10 |
| Port 2 | Open | 2 | 0.00824 | 0.60 | 0.40 | 1.62 | 0.58 | 1.00 | 0.09 | 0.04 | 0.39 | 0.89 | 0.24 |
| | | 4 | 0.01264 | 0.70 | 0.30 | 1.99 | 0.93 | 1.00 | 0.05 | 0.03 | 0.10 | 0.99 | 0.08 |
| | | 6 | 0.01402 | 0.78 | 0.22 | 2.25 | 1.09 | 1.00 | 0.02 | 0.03 | 0.04 | 0.98 | 0.18 |
| | | 8 | 0.01424 | 0.84 | 0.16 | 2.68 | 2.34 | 1.00 | 0.07 | 0.01 | 0.35 | 0.90 | 0.27 |
| | | 10 | 0.01556 | 0.82 | 0.18 | 3.04 | 2.58 | 0.99 | 0.14 | 0.03 | 0.36 | 0.92 | 0.17 |
| | Close | 8 | 0.01362 | 0.75 | 0.25 | 2.53 | 1.66 | 0.99 | 0.10 | 0.03 | 0.20 | 0.98 | 0.04 |
| | | 6 | 0.01152 | 0.71 | 0.29 | 2.21 | 1.44 | 1.00 | 0.05 | 0.04 | 0.16 | 0.99 | 0.03 |
| | | 4 | 0.00832 | 0.69 | 0.31 | 1.99 | 1.22 | 1.00 | 0.01 | 0.05 | 0.09 | 0.99 | 0.13 |
| | | 2 | 0.00417 | 0.67 | 0.33 | 1.75 | 0.77 | 1.00 | 0.04 | 0.05 | 0.00 | 0.95 | 0.32 |

**Table II.**
Flow directional coefficients from conventional (Port 1) and tumble (Port 2) ports for full load and engine speed of 1,500 rpm

closer to 1 for all the valve lifts, $C_{1y}$ and $C_{1z}$ being negligible. For the same valve lifts, coefficient $C_{1m}$ during the valve closing is smaller than during the valve opening, which shows the inertial behaviour of the flow. In opposition, a much more homogeneous distribution is found in the zone 2. The main flow is oriented through the $y$ direction but the other components have a significant fraction of the total mass flow rate. The $x$ and $y$ components (characterized by $C_{2x}$ and $C_{2y}$, respectively) are opposite to the tumble vortex generated by $C_{1x}$. On the other hand the $z$-component of the flow, being related to the swirl motion, has no direct influence in the tumble motion.

The asymmetrical flow distribution characterized by the coefficients in Table II is pointed out by tracing the $C_{1m}$ values along with all the valve movement (opening and closing). Figure 9 shows it for both port and several operative conditions. Engine speed and load levels do not seem to have a strong influence over flow distribution around valve curtain. For both ports, the asymmetrical flow distribution grows while valve lift increases. Highest $C_{1m}$ values are found during valve opening close to 8 mm of valve lift. For the highest engine speed the flow inertia enhances the imbalance during high-valve lifts for the tumble port. But, it does not seem to occur for the conventional port (Figure 10).

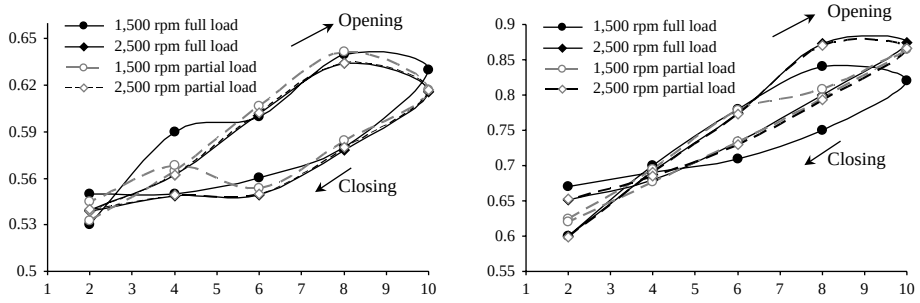


**Figure 10.**
$C_{1m}$ coefficient along opening and closing valve movement; left: conventional port; right: tumble port

Similar flow behaviour is found for the rest of the set coefficients for all engine conditions analyzed.

Figure 11 shows the $x$ component of the flow over three vertical lines inside the cylinder. As for the conventional port (at the top of the figure), the tumble vortex is not clearly defined at any time. The velocity field near the cylinder wall has a unique direction along the wall, which is consistent with the swirl momentum $J_{ny}$ reported in Figure 6. Tumble motion takes place only near the cylinder axis and it quickly diminishes when the valve starts closing.

For the tumble port (Figure 11 at bottom), it can be seen that the tumble vortex is defined since the first stages of the intake period (around 70° CA ATDC), and it takes place along the whole domain. The tumble-vortex axis is located near the piston head during the intake period but it approaches the cylinder centre while the piston goes up. The vortex holds a definite shape even during the last stages of the compression stroke. It is well in agreement with quantitative results in Figure 5.

Figure 12 helps to understand the complexity of the flow patterns originated inside the cylinder. In it, the velocity fields over planes parallel to the cylinder mean plane are shown for both ports at $\varphi = 256°$ CA ATDC.

The differences in the tumble motion generated in each port also have consequences over the turbulence quantities. The motion of large-scale flow structures has less-energy dissipation rate and accordingly favours the accumulation of entering kinetic energy. When these flow structures take place along the whole domain, they can last to the end of the compression stroke. Figure 13 shows the velocity field for the

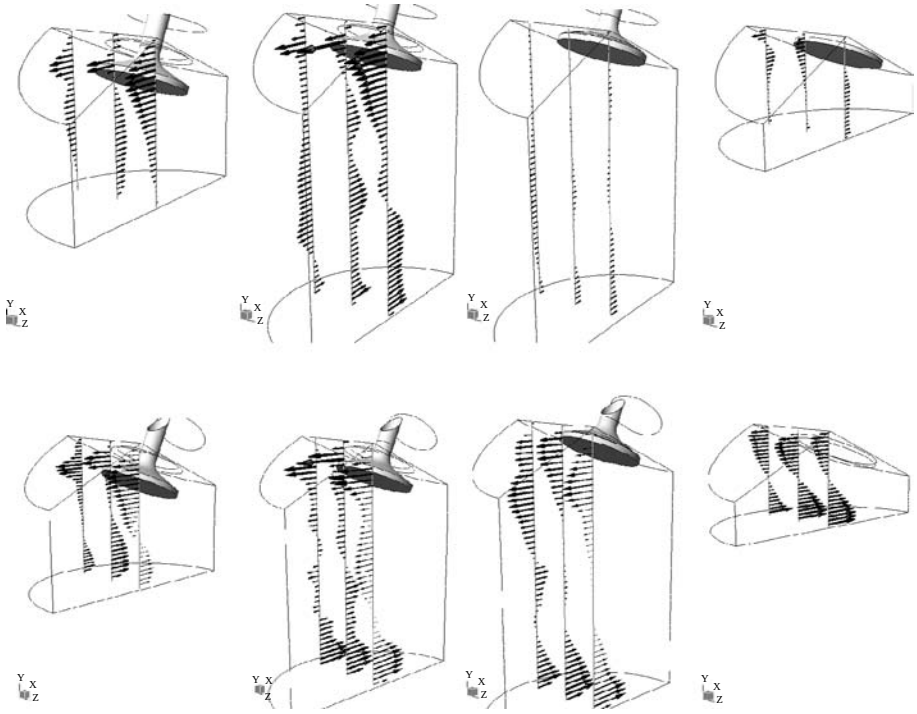

**Figure 11.**
Velocity field inside the cylinder (full load and engine speed of 1,500 rpm) at $\varphi = 72$, 144, 216 and 324° CA ATDC; upper: conventional port; bottom: tumble port

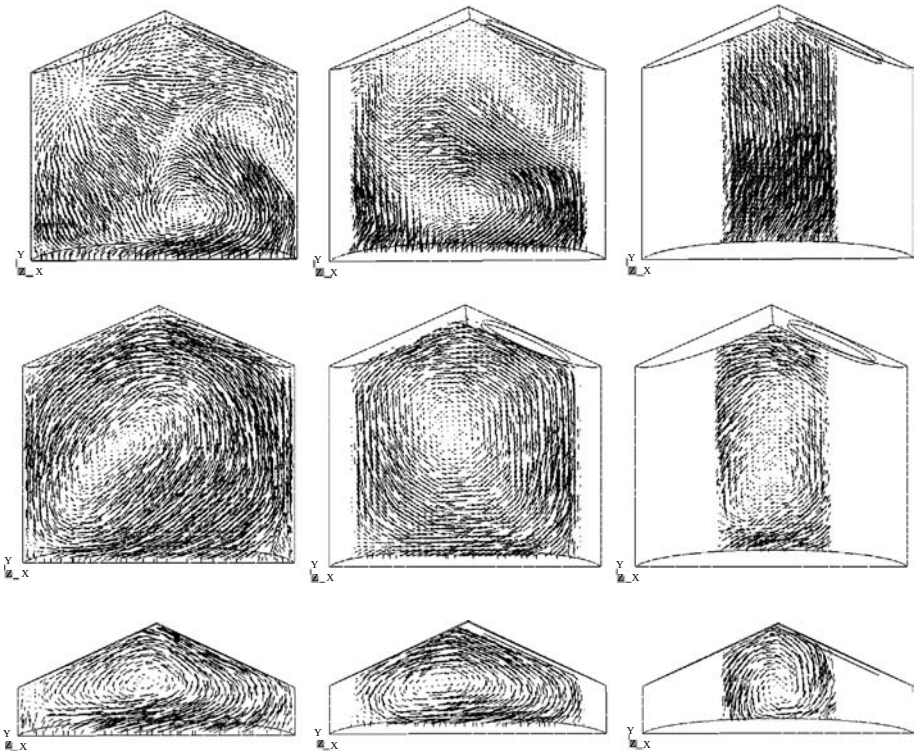

**Notes:** Left: cylinder mean plane; Centre: valve mean plane; Right: ¾ of cylinder radius from cylinder mean plane

**Figure 12.**
Velocity field over *x-y* planes (upper: conventional port, bottom: tumble port) at 252° CA ATDC (full load and engine speed of 1,500 rpm); left: cylinder mean plane; centre: valve mean plane; right: 3/4 of cylinder radius from cylinder mean plane

**Figure 13.**
Velocity field over *x-y* planes for tumble port at 324° CA ATDC (full load and engine speed of 1,500 rpm)

tumble port at three different planes parallel to the cylinder mean plane before ending the compression stroke. It may be noted how the tumble vortex is kept the compression notwithstanding. Of course, during the compression stroke the piston goes up and the frictional stresses increase due to the vortex distortion. At the end of the compression stroke this phenomenon produces a degradation of the tumble vortex turning the kinetic energy of the mean flow in turbulent kinetic energy.

The spatial-averaged turbulence intensity $u'$ is drawn in Figure 14. It shows how the tumble port may highlight the increment of turbulent kinetic energy just mentioned.

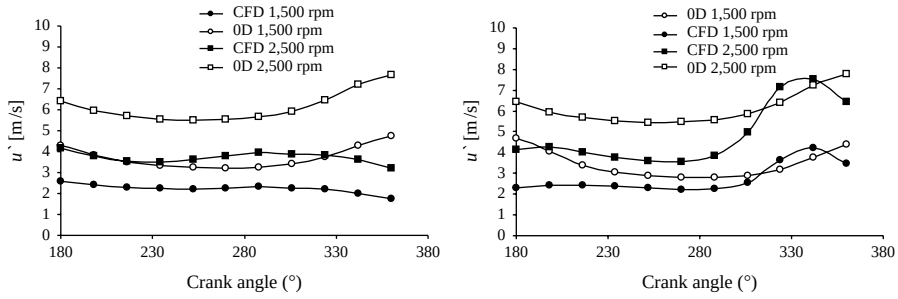


**Figure 14.**
Turbulence intensity $u'$ along the compression stroke for both port configurations (full load); left: conventional port; right: tumble port

For the conventional port, the 0-D model gives a marked overestimation of turbulence intensity at the end of the compression stroke.

The combustion flame speed is highly dependent on the unburned mass entrainment, which being closely related to its mixture capability through the turbulent kinetic energy, makes the local distribution of the turbulence intensity in the vicinity of the spark plug crucial.

Figure 15 shows the $u'$ spatial averaged for the whole cylinder and inside three different spheres (of radius $r = 5$, 10 and 15 mm), centred in the spark plug.

Only for the tumble port a stronger correlation among the four curves is found. That means the turbulence levels are more homogeneous along the whole cylinder, giving more realism to the 0-D model approach.

*0D-model modifications*

According to Figure 12, the tumble port configuration seems to be more adequate for the hypothesis of a velocity field represented by an almost rigid body rotation. By analyzing the underestimation on the entering tumble momentum obtained for the tumble port and taking into account the zonal analysis of the incoming mass flow rate presented above, it was reasonable to propose a modification on the 0-D model, in order to improve it. The change was focused over the entrance-momentum quantity (equation (2)), which was reformulated considering the entrance-flow distribution around the valve curtain. Only three ($\theta_{1x}$, $\theta_{2x}$ and $\theta_{2y}$) of the six flow components were taken into account (see Figure 9 at right). Then, the new expression for the entrance tumble momentum was:

$$\frac{\mathrm{d}J_{\mathrm{in}}}{\mathrm{d}t} = \sum_{i=1}^{n} \dot{m}_i \bar{v}_i r_i = \dot{m}_1 \bar{v}_{1x} \cdot r_1 - \dot{m}_2 \bar{v}_{2x} \cdot r_2 - \dot{m}_2 \bar{v}_{2y} \cdot r_3, \tag{23}$$

where $r_1$, $r_2$ and $r_3$ are the distances from the vortex centre to each one of the three considered entering flow components ($\theta_{x1}$, $\theta_{x2}$ and $\theta_{y2}$). $r_1$ and $r_2$ are taken equal to $h$ and $r_3$ is half the cylinder radius.

The results obtained with this modification along with the original 0-D model ones and the corresponding CFD results for both port configurations are shown in Figure 16.

Although the conventional port prediction from the 0-D model is far from being reliable because of the model hypotheses previously explained, the over estimation obtained with the original 0-D model along the intake stroke was corrected by using the modified one. This improved the predicted tumble conditions for the compression stroke, as can be seen from Figure 16. However, as the modification influences only the

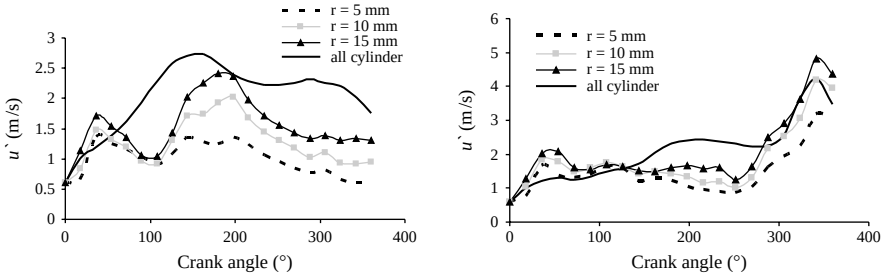


**Figure 15.**
Averaged turbulence intensity $u'$ (CFD results) close to the spark plug and in the whole cylinder (engine speed 1,500 rpm); left: conventional port; right: tumble port

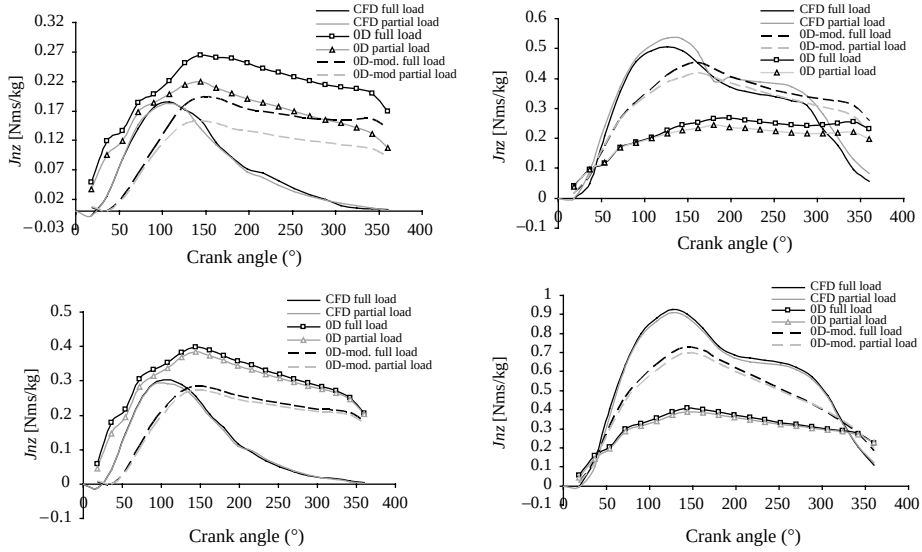


**Figure 16.**
Normalized tumble momentum $J_{nz}$ from the original 0-D model, the modified 0-D model and CFD (left: conventional port, right: tumble port). Upper: engine speed of 1,500 rpm; bottom: engine speed of 2500 rpm

intake period, it has no influence on the tumble evolution during the compression period.

As regards the tumble port, the modified 0-D model gives a better estimation than the original one during both strokes. The explanation about how the modified 0-D model generates more tumble momentum than the original one is found in the increased velocity (and also momentum) achieved by the entering flow through the zone 1 in Figure 9. Such a difference may be justified even taken into account that the original 0-D model considers that all the entering flow producing positive tumble motion.

By looking at $C_{1v}$ and $C_{2v}$ coefficients in Table II ($C_{1v}$ and $C_{2v}$ coefficients relate $v_1$ and $v_2$ velocities to the mean inlet normal velocity $v_n$) it is clear that the flow through each curtain zone can take velocities higher than the inlet mean velocity $v_n$. It is important to note that due to the nature of the mass flow rate average used in this analysis, the flow velocities $v_1$ and $v_2$ can assume values larger than $v_n$ at the same time. In fact, the flow entering through the zone 1 takes velocity values larger than $2v_n$ for valve lifts higher than 4 mm. Summarizing, the mass flow rate average takes into account the effective entering flow area in each zone and the consequent increment of the flow acceleration. So, in spite of only a fraction of the overall inlet flow (given by $C_{1m}$ coefficient) generates positive tumble movement, the entering momentum flow is increased by a local acceleration on the valve curtain.

As for the turbulence intensity both the 0-D model and the modified one give bad estimations during the whole strokes. Model changes have not appreciable effects over the turbulence predictions.

Finally, it should be emphasized that at the current state of this work the proposed velocity correction at intake should not be understood as a model; it is only a strategy to assess how the 0-D model enhanced with additional information may reproduce the CFD results in a better way.

## Conclusion

A 0-D model for tumble estimation in four-valve pentroof engines was implemented. The results from this model were compared to those obtained by CFD simulations for two different intake port configurations, which lead to the following conclusions:

- The 0-D model estimations show strong differences with respect to CFD results.
- The 0-D model should be used only for high-tumble port configuration engines where the model hypotheses are valid, in particular those related to the imposed velocity field.
- The 0-D model underestimates the entering tumble momentum for port configurations which promote tumble motion.
- The 0-D model overestimates the turbulence intensity during both strokes.
- Even though experimental measurements and CFD results proved to be very sensitive to changes in the intake port configuration, the 0-D model does not follow this tendency. The 0-D model requires better characterization of the incoming flow because of its great influence on the tumble generation.
- CFD results show to be not strongly affected by in-cylinder load levels. Besides, the entering flow patterns around valve curtain seem to be very similar for different load levels and engine speed analyzed.
- Differences between CFD and 0-D model estimations grow up while engine speed increases.
- This study shows that potential improvement in the model prediction is only feasible when extra information about the incoming flow is added and it is applied to high-tumble engines.

## References

Achuth, M. and Metha, P.S. (2001), "Predictions of tumble and turbulence in four-valve pentroof spark ignition engines", *International Journal of Engine Research*, Vol. 2 No. 3, pp. 209-27.

Aleiferis, P.G., Taylor, A.M.K.P., Ishii, K. and Urata, Y. (2004), "The nature of early flame development in a lean-burn stratified-charge spark-ignition engine", *Combustion and Flame*, Vol. 136, pp. 283-302.

Benjamin, S.F. (1993), "Prediction of barrel swirl and turbulence in reciprocating engines using a phenomenological model", IMechE, Paper L20/C465-013, pp. 87-101.

Huang, R.F., Huang, C.W., Chang, S.B., Yang, H.S., Lin, T.W. and Hsu, W.Y. (2005), "Topological flow evolutions in cylinder of a motored engine during intake and compression strokes", *Journal of Fluid and Structures*, Vol. 20, pp. 105-27.

Johan, Z., Moraes, C.M., Buell, J.C. and Ferencz, R.M. (2001), "In-cylinder cold flow simulation using a finite element method", *Computer Methods in Applied Mechanics and Engineering*, Vol. 190, pp. 3069-80.

Kang, K.Y. and Baek, J.H. (1995), "LDV measurement and analysis of tumble formation and decay in a four-valve engine", *Experimental Thermal and Fluid Science*, Vol. 11, pp. 181-9.

Kang, K.Y. and Baek, J.H. (1998), "Turbulence characteristics of tumble flow in a four-valve engine", *Experimental Thermal and Fluid Science*, Vol. 18, pp. 231-43.

Lee, K., Lee, C. and Joo, Y. (2001), "Optimization of the intake port shape for a five-valve gasoline engine", *Journal of Automotive Engineering*, Vol. 215 No. 6, Part. D, pp. 739-46.

Li, Y., Liu, S., Shi, S.X., Feng, M. and Sui, X. (2001a), "An investigation of in-cylinder tumbling motion in a four-valve spark ignition engine", *Journal of Automotive Engineering*, Vol. 215 No. 2, Part. D, pp. 273-84.

Li, Y., Zhao, H., Leach, B. and Ma, T. (2003), "Charge stratification in a strong tumble SI engine", Technical Report, Brunel University, Brunel.

Li, Y., Zhao, H., Peng, Z. and Ladommatos, N. (2001b), "Analysis of tumble and swirl motions in a four-valve SI engine", SAE, Paper 2001-01-3555.

McLanddress, A., Emerson, R., McDowell, P. and Rutland, C. (1996), "Intake and in-cylinder flow modeling characterization of mixing and comparison with flow bench results", SAE, Paper 960635.

Poulos, S.G. and Heywood, J.B. (1983), "The effect of chamber geometry on spark-ignition engine combustion", SAE, paper 830334.

Ramajo, D., Zanotti, A. and Nigro, N. (2005), "Estimación de la turbulencia en cámaras de combustión y su incidencia en la velocidad de avance de llama", paper presented at MECOM 2005.

Seeley, W.A. (1998), "A predictive study of barrel swirl flow in a spark ignition engine using computational fluid dynamics", PhD thesis, Coventry University, Coventry.

## Further reading

Heywood, J.B. (1988), *Internal Combustion Engine Fundamentals*, McGraw-Hill, New York, NY.

**Corresponding author**
Damian Ramajo can be contacted at: dramajo@ceride.gov.ar